Application of a particle, momentum, and energy balance model to calculate the structure of the edge pedestal in DIII-D

W. M. Stacey
Fusion Research Center, Georgia Institute of Technology, Atlanta, Georgia 30332

R. J. Groebner
Fusion Division, General Atomics, San Diego, California 92186

(Received 9 November 2004; accepted 5 January 2005; published online 17 March 2005)

A calculation of edge density and temperature profiles based on "classical" physics—particle, momentum, and energy balances, heat conduction closure relations, and neutral particle transport—yielded a pedestal structure that is qualitatively and quantitatively similar to that found experimentally in five DIII-D [J. Luxon, Nucl. Fusion **42**, 614 (2002)] discharges, when experimental radial electric field and rotation profiles and experimentally inferred heat transport coefficients were used. The principal cause of the density pedestal was a peaking of the inward pinch velocity just inside the separatrix caused by the negative well in the experimental electric field, and the secondary cause was a peaking of the radial particle flux caused by the ionization of incoming neutrals. There is some evidence that this peaking of the radial particle flux just inside the separatrix may also be responsible in part for the negative electric field in that location. © *2005 American Institute of Physics*. [DOI: 10.1063/1.1864066]

I. INTRODUCTION

The "pedestal" structure of the density and temperature profiles in the edge of H-mode plasmas has been the subject of intensive research for a number of years (see Ref. 1 for review). This interest is motivated in part by the recognition that core transport calculations of the performance of future fusion reactors depend sensitively on the value of the pedestal density and, in particular, the pedestal temperature used as boundary conditions in these calculations.[2,3]

Many pedestal investigations have focused on understanding the magnetohydrodynamic (MHD) instabilities that limit the pressure or pressure gradient in the edge pedestal (e.g., Refs. 4–9) or on identifying the experimental relations among MHD instability parameters, device operating parameters, and pedestal parameters (e.g., Refs. 10–13). Correlations of measured pedestal density and temperature values and pedestal profile widths with various MHD and plasma operating parameters have led to theory-based empirical scaling laws (e.g., Ref. 14).

While the MHD instabilities that limit the edge pressure and pressure gradients have been the subject of the majority of the investigations to date, there also have been both (i) studies of transport (e.g., Refs. 15 and 16) and other (e.g., Refs. 17–19) mechanisms that could cause the formation of the H-mode pedestal and (ii) studies of the causes of the observed pedestal structure—widths and gradients of the density and temperature profiles—(e.g., Refs. 20–27). The importance of the ionization of recycling neutrals and of the formation of a negative radial electric field well in determining the edge pedestal structure has been suggested by several of these authors. Also, the pedestal is modeled in many sophisticated edge and core plasma calculations (e.g., Refs. 28–30) by adjusting transport coefficients in the particle and energy balance equations to obtain agreement with experimental profiles.

This paper reports an examination of the recently suggested possibility[26,27] that the edge pedestal structure can be understood entirely (excepting the transport coefficients) as a consequence of the requirements of "classical" particle, momentum, and energy balance plus the heat conduction relation, in the presence of recycling neutrals. (The word classical, as used in this paper, refers to the first three-fluid moment equations plus the heat conduction closure relation, but not necessarily to the use of neoclassical or any other particular theory for the transport coefficients.) One notable feature of the theory to be tested is that the particle flux-gradient-pinch relation is derived directly from the momentum balance equations, making it unnecessary to externally specify a diffusion coefficient and a pinch velocity. Since only the first three moment equations are used and the heat conduction relation is imposed as a closure relation, it is necessary to specify the heat conduction coefficients external to the basic calculation. Similarly, it is necessary to specify a radial momentum transport coefficient external to the basic calculation. These transport coefficients are inferred *ab initio* from the experimental data in this paper.

The calculation[26,27] that is tested in this paper is as follows. The particle and heat balance equations are numerically integrated inward from the separatrix, using separatrix boundary conditions determined from overall energy and particle balances on the plasma within the separatrix, to obtain profiles of the heat (Q) and particle (Γ) fluxes in the plasma edge. The neutral densities needed to evaluate the atomic physics particle sources and heat losses are calculated with a 2D transport model. The heat conduction relations for ions and electrons, $q=(Q-2.5\Gamma T)=nT\chi L_T^{-1}$ are used to determine the radial profile of L_T^{-1}, and then the definitions $-(dT/dr)/T=L_T^{-1}=(Q-2.5\Gamma T)/nT\chi$ are integrated radially

inward from the separatrix, using experimental separatrix temperature boundary conditions, to calculate the ion and electron temperature profiles.

The momentum balance equations are solved for the requirement $L_p^{-1}=-(dp/dr)/p=(v_r-v_{pinch})/D$, where v_{pinch} denotes a collection of terms involving the radial electric field E_r, the toroidal and poloidal rotation velocities, v_φ and v_θ, the frequency v_d^* for the radial transfer of toroidal momentum, and the toroidal components of the beam momentum input and the induced electric field. The radial electric field and the carbon toroidal and poloidal rotation velocities used in the evaluation of v_{pinch} are taken from experiment. The quantity D denotes another collection of terms arising, as v_{pinch} does, from the derivation of the relation for L_p^{-1} from momentum balance. The ion density profile is calculated by numerically integrating $-(dn/dr)/n=L_n^{-1}=L_{pi}^{-1}-L_{Ti}^{-1}=(v_r-v_{pinch})/D-L_T^{-1}$ inward from the separatrix, using an experimental separatrix density boundary condition.

This coupled nonlinear set of equations is iterated to obtain a converged solution for the radial profiles of density, ion and electron temperatures, particle and heat fluxes, and neutral density in the edge plasma. Thus, these profiles are the consequence of classical particle, momentum, and energy balances, and the heat conduction relation in the presence of recycling neutrals, given the boundary conditions, transport coefficients, and radial electric field and the carbon toroidal and poloidal rotation velocities inferred or taken from experiment. Comparison of these profiles with the directly measured experimental density and temperature profiles thus provides a test of whether those profiles can be understood in terms of classical physics—particle, momentum, and energy balance plus the heat conduction relation—with the exception that the transport coefficients and the radial electric field and rotation velocities taken from experiment may be produced in part by "nonclassical," or anomalous, effects.

It is possible to extend the investigation to remove these exceptions. The radial electric field and the rotation velocities also can be calculated from classical physics—momentum balance—and thus to extend the test of the ability to understand pedestal structure in terms of classical physics. This is done for one of the discharges considered, but a full investigation remains the subject of a future paper.

This calculation model is described in detail in Sec. II, the calculated edge profiles are compared with measured profiles for five DIII-D discharges in Sec. III, the calculation is discussed vis-à-vis related work in Sec. IV, and the results are summarized and conclusions are presented in Sec. V.

II. CALCULATION MODEL

The calculation model was derived[26,27] from fluid particle, momentum, and energy balance plus the heat conduction closure relation.

A. Radial particle and heat balances

The local flux surface averaged particle balance equation for the main ion particle flux in the edge plasma can be written as

$$\frac{d\Gamma_i}{dr}=n_e\nu_{ioni}+n_i\nu_{ionb},\quad \Gamma_i(r_{sep})=\Gamma_i^{sep}, \tag{1}$$

where ν_{ioni} and ν_{ionb} are the frequencies for the ionization by electron impact of recycling or fueling neutral atoms of the main ion species and for ionization of neutral beam injected particles, respectively. This equation is integrated numerically inward from the separatrix, where the (net outward) ion particle flux crossing the separatrix Γ_{sepi} is specified as the boundary condition.

The ion and electron heat fluxes in the edge region satisfy the energy balance equations

$$\frac{dQ_i}{dr}=-\frac{3}{2}T_in_e\nu_{ati}-\dot{Q}_{ie}+\dot{Q}_{nbi},\quad Q_i(r_{sep})=Q_i^{sep} \tag{2}$$

and

$$\frac{dQ_e}{dr}=-E_{ion}n_e\nu_{ioni}-n_en_zL_z+\dot{Q}_{ie}+\dot{Q}_{n_{be}},$$
$$Q_e(r_{sep})=Q_e^{sep}, \tag{3}$$

where $\dot{Q}_{ie}$ is the rate of collisional energy transfer from ions to electrons, $\dot{Q}_{nbi,e}$ is the rate of energy deposition in the ions or electrons by injected neutral beams (or any other form of heating), ν_{ati} is the frequency of charge exchange plus elastic scattering of cool recycling neutral atoms which have not previously suffered a collision in the scrape-off layer (SOL) or edge region, E_{ion} is the ionization energy, and L_z is the radiation emissivity of the impurity ions (which is calculated with a coronal equilibrium model using the local electron density and temperature, taking into account the enhancement due to charge exchange and recombination with the recycling neutrals). The values of the outward ion and electron heat fluxes at the separatrix are specified as boundary conditions, and these equations are numerically integrated inward from the separatrix into the edge region.

The outward ion flux Γ_i and the total heat flux at the separatrix, $Q^{sep}=Q_i^{sep}+Q_e^{sep}$, can be determined from particle and power balances on the region inside the separatrix. The split between ion and electron heat fluxes is generally not known experimentally and must be estimated.

B. Pressure and temperature gradient scale lengths

It was shown previously[26,27] that the parallel and radial components of the momentum balance equations for a multispecies tokamak plasma can quite generally be solved to obtained a coupled set of equations relating the pressure gradients, the particle fluxes, the radial electric fields, the rotation velocities, and certain other terms. When it is assumed that (i) the plasma contains a main ion species "i" and a single effective impurity species "z" the concentration of which is a constant fraction $f_z=n_z/n_i$ of the main ion concentration, and that (ii) both ion species have the same temperature T_i, these equations reduce to a flux-gradient-pinch relationship for the main ions that constrains the inverse pressure gradient scale length

$$-\frac{1}{p_i}\frac{dp_i}{dr} \equiv L_{pi}^{-1} = \frac{\Gamma_i/n_i - v_{pi}}{\hat{D}_i} \equiv \frac{v_{ri} - v_{pi}}{\hat{D}_i}. \quad (4)$$

The quantity D_i is a collection of terms arising in the derivation that has the form of an effective diffusion coefficient

$$\hat{D}_i \equiv D_{ii} - D_{iz} = \frac{m_i T_i \nu_{iz}}{(e_i B_\theta)^2}\left[1 + \frac{\nu_{di}^*}{\nu_{iz}} - \frac{1}{\langle Z\rangle}\right], \quad (5)$$

where ν_{iz} is the interspecies collision frequency, ν_{di}^* is the viscous plus atomic physics (charge exchange, elastic scattering, and ionization) frequency for the removal of toroidal momentum, and $\langle Z\rangle$ is the average local charge state of the impurity species. The remaining quantities entering this relationship can be collected and identified as the "pinch" velocity

$$v_{pi} = \frac{1}{e_i B_\theta}[-M_{\phi i}/n_i - e_i E_\phi^A + m_i \nu_{di}^*(E_r/B_\theta + f_p^{-1} v_{\theta i}) + m_i \nu_{iz} f_p^{-1}(v_{\theta i} - v_{\theta z})], \quad (6)$$

where M_φ and E_φ^A are the toroidal components of the input momentum rate and the induced electric field, E_r is the radial electric field, v_θ is the poloidal rotation velocity, and $f_p = B_\theta/B_\varphi$.

It is emphasized that all quantities in Eqs. (4)–(6) arose directly from the requirements of radial and parallel momentum balances and particle balance. The identification of a diffusion coefficient and a pinch velocity is a notational convenience.

The local heat conduction relation $q_j = -n_j \chi_j dT_j/dr$, $j = i,e$, can be used to express the local ion and electron inverse temperature gradient scale lengths, $L_{Tj}^{-1} \equiv -(dT_j/dr)/T_j$, in terms of the respective local total heat fluxes Q_j and convective heat fluxes $5/2 T_j \Gamma_j$:

$$L_{Tj}^{-1} = \frac{1}{\chi_j}\left[\frac{Q_j}{n_j T_j} - \frac{5}{2}\frac{\Gamma_j}{n_j}\right], \quad j = i,e. \quad (7)$$

C. Density and temperature profiles

The ion density profile and the ion and electron temperature profiles in the plasma edge are calculated by numerically integrating the defining relations for the respective inverse gradient scale lengths inward from the separatrix

$$-\frac{1}{n_i}\frac{dn_i}{dr} = L_{ni}^{-1} = L_{pi}^{-1} - L_{Ti}^{-1} = \frac{v_{ri} - v_{pi}}{\hat{D}_i} - L_{Ti}^{-1},$$

$$n_i(r_{sep}) = n_i^{sep}, \quad (8)$$

$$-\frac{1}{T_i}\frac{dT_i}{dr} = L_{Ti}^{-1} = \frac{1}{\chi_i}\left[\frac{Q_i}{n_i T_i} - \frac{5}{2}\frac{\Gamma_i}{n_i}\right], \quad T_i(r_{sep}) = T_i^{sep}, \quad (9)$$

and

$$-\frac{1}{T_e}\frac{dT_e}{dr} = L_{Te}^{-1} = \frac{1}{\chi_e}\left[\frac{Q_e}{n_e T_e} - \frac{5}{2}\frac{\Gamma_e}{n_e}\right], \quad T_e(r_{sep}) = T_e^{sep} \quad (10)$$

subject to separatrix boundary conditions taken from experiment in this paper.

The local values of the heat and particle fluxes calculated from Eqs. (1)–(3) must be used in solving Eqs. (8)–(10), and conversely the local values of n and T obtained by solving Eqs. (8)–(10) are needed in order to solve Eqs. (1)–(3) for Γ and Q.

D. Neutral density profiles

Penetration of the inward flux of recycling neutrals $J^+(r)$ into the edge region is calculated using an interface-current-balance method,[31] using as a boundary condition the recycling neutral current $J^+(r_{sol}) = J_{sol}^+$, passing inward across the outer boundary of the SOL. The inward $(+)$ and outward $(-)$ partial currents at successive interfaces r_n and r_{n+1} are related by

$$J_+(r_{n+1}) = T_n J_+(r_n) + R_n J_-(r_{n+1}),$$
$$J_-(r_n) = T_n J_-(r_{n+1}) + R_n J_+(r_n), \quad n = 1,2,\ldots,N, \quad (11)$$

where T_n is the probability that a neutral atom is transmitted through the interval $\Delta_n = r_{n+1} - r_n$ without a collision and $2R_n$ is the probability that a neutral atom (or its neutral progeny via charge exchange) that does have one or more collisions in the interval Δ_n ultimately escapes from the interval across the interface at r_n or r_{n+1}. These quantities are defined in Ref. 31. The inward neutral current across the scrape-off layer is calculated with a two-dimensional (2D) model of the recycling of plasma ions from the divertor plate and their transport through the divertor plasma, private flux, and edge plenum regions using the transmission-escape probabilities method.[32]

Two groups of neutrals are treated: (i) "cold" neutrals which have recycled from the wall and penetrated across the SOL and into the plasma edge with a temperature characteristic of the wall recycling atoms and (ii) neutrals that have undergone one or more charge-exchange or scattering collisions in the SOL or pedestal regions and taken on the local ion temperature as a result. The first group of neutrals is used to compute the cold neutral density that is used to evaluate ν_{ati}, while both groups contribute to ν_{ioni}.

This neutral transport computation has been checked against neutral density measurements in DIII-D and Monte Carlo calculations of these experiments.[33] The neutral densities in the plasma edge near the X-point were measured[34] using a 2D reconstruction of D_α light at the divertor Thomson scattering locations. This experiment was modeled in detail for a Monte Carlo calculation and using the same procedure as used for the neutral calculation in this paper. The agreement between both calculations and the measured neutral densities was good. A recent summary of the neutral calculation used in this paper can be found in Ref. 33.

E. Boundary conditions for edge profile calculations

As stated above, the separatrix density and temperature boundary conditions for Eqs. (8)–(10) are taken directly from experimental measurement, and the incident neutral flux boundary condition for Eqs. (11) is calculated with a 2D neutral fueling and recycling code.

The outward particle and heat flux separatrix boundary conditions for Eqs. (1)–(3) are obtained from particle and heat balances on the plasma inside of the separatrix, including the neutral influx, the neutral beam heat, and particle sources and the radiative losses from within the separatrix. For this purpose we have embedded the above edge plasma calculation within a global code,[35] which (i) performs core plasma particle and power balance calculations (including radiative cooling and recyling neutral influx) to determine outward plasma particle and heat fluxes across the separatrix into the SOL, which (ii) are input for a "two-point" divertor model (including radiative and atomic physics cooling, particle sources, and momentum sinks) to calculate plasma density and temperature on the separatrix at the midplane and at the divertor plate and to calculate the plasma flux to the divertor plate, which (iii) creates the recycling source of neutral molecules and atoms for a 2D neutral transport recycling calculation throughout the divertor and plasma chamber that provides the neutral influx for the core particle balance calculation.

F. Rotation velocities and radial electric field

Evaluation of the pinch velocity of Eq. (6) requires an evaluation of the rotation velocities and the radial electric field. The toroidal and poloidal rotation velocities for carbon, $v_{\varphi c}^{expt}$ and $v_{\theta c}^{expt}$, that are measured experimentally, and the "experimental" radial electric field that is constructed from these measured velocities and the measured carbon pressure gradient L_{pc}^{-1} by using the radial momentum balance

$$E_r/B_\theta + v_{\theta j} f_p^{-1} = v_{\varphi j} - T_j L_{pj}^{-1}/e_j B_\theta \tag{12}$$

are used to evaluate the pinch velocity.

The poloidal velocity for the main ions $v_{\theta i}$ is evaluated from using poloidal momentum balance[26,27,36] to calculate the difference $(v_{\theta i} - v_{\theta c})_{calc}$ which is then used with the experimental $v_{\theta c}^{expt}$ to construct an experimental $v_{\theta i}^{expt} = v_{\theta c}^{expt} + (v_{\theta i} - v_{\theta c})_{calc}$. A value for $v_{\varphi i}$ for the main ions is needed in the poloidal momentum balance that is used to calculate $(v_{\theta i} - v_{\theta c})_{calc}$. An experimental value for this quantity is constructed from $v_{\varphi i}^{expt} = v_{\varphi c}^{expt} + (v_{\varphi i} - v_{\varphi c})_{calc}$, where the difference $(v_{\varphi i} - v_{\varphi c})_{calc}$ is determined by subtracting Eqs. (12) for the two species.

G. Transport coefficients inferred from experiment

The transport coefficients used in the calculations were inferred from experiment. Average values of $L_{Ti,e}^{-1}$ were determined from the endpoint measured temperature values (1) over the steep gradient region and (2) over the region immediately inward from the top of the pedestal, and corresponding average experimental values $\chi_{i,e} = (Q_{i,e} - 2.5\Gamma T_{i,e})/nT_{i,e}L_{Ti,e}^{-1}$ were constructed for each region and used in the calculations. The profiles of the experimental momentum transfer frequencies v_{dj}^* for carbon and deuterium were inferred from the toroidal momentum balance equations, which are balances between momentum input and transfer rates, using the experimental values of the toroidal rotation velocities and the known momentum input rates to obtain

$$\begin{aligned} \nu_{di}^* = \{ & M_{\varphi i} + n_i e_i E_\varphi^A + n_i m_i \nu_{iz} [f_p^{-1}(v_{\theta i} - v_{\theta z}) + T_i L_{pi}^{-1}/e_i B_\theta (1 \\ & - 1/\langle Z \rangle)] \div n_i m_i \nu_{iz} [v_{\varphi z} + f_p^{-1}(v_{\theta i} - v_{\theta z}) \\ & + T_i L_{pi}^{-1}/e_i B_\theta (1 - 1/\langle Z \rangle)]\} \end{aligned} \tag{13}$$

for the main ions and

$$\begin{aligned} \nu_{dz}^* = \{ & M_{\varphi z} + n_z e_z E_\varphi^A + n_i m_i \nu_{iz} [f_p^{-1}(v_{\theta i} - v_{\theta z}) \\ & + T_i L_{pi}^{-1}/e_i B_\theta (1 - 1/\langle Z \rangle)] \div n_z m_{z\nu} v_{\varphi z}\} \end{aligned} \tag{14}$$

for the carbon impurity ions ($z=c$). The experimental rotation velocities discussed above are used to evaluate these expressions as a function of radial position in the edge plasma.

H. Solution procedure

First, the plasma is modeled with the global code[35]—particle and power balances on the core plasma, two-point divertor model, and 2D recycling neutral calculation—described in Sec. II E, which calculates the separatrix boundary conditions on the outward particle and power fluxes (Γ_i^{sep} *and* $Q_{i,e}^{sep}$) needed for Eqs. (1)–(3) and the scrape-off layer boundary condition on inward neutral flux J_{sol}^+ needed for Eq. (11). Experimental results are used to ensure that the correct plasma edge temperature and density conditions are used in the neutral fueling calculation. The plasma edge transport coefficients are inferred from experimental edge data and the experimental separatrix boundary conditions on density and temperature ($n_i^{sep}, T_{I,e}^{sep}$) needed for Eqs. (8)–(10) are set at this stage.

Next, the nonlinear set of coupled ordinary differential Eqs. (1)–(3), (8)–(10) and the neutral current balance Eqs. (11) are solved iteratively for the radial profiles of Γ_i^{sep}, $Q_{i,e}^{sep}$, n_i^{sep}, $T_{i,e}^{sep}$, and n_o. The numerical integration is carried out on a finite-difference grid using 25 mesh points extending from the separatrix ($\rho=1.0$) into the plasma to $\rho \approx 0.86$. The auxiliary evaluations of D and v_{pinch} are updated at each mesh point on each iteration. The iterative solution is converged to 10^{-4} at all mesh points on successive iterates of densities, temperatures, and particle and heat fluxes.

III. COMPARISON OF CALCULATED AND MEASURED DIII-D EDGE PROFILES

The profiles of density and temperatures calculated above were compared against measured density and temperature profiles. Five DIII-D shots with rather different plasma and pedestal parameters, as indicated in Table I, were chosen for the comparison of calculated and measured (Thomson scattering and CER) density and temperature profiles. The quantity Γ_{neut}^{in} is the total fueling and recycling neutral influx rate across the separatrix (not including the neutral beams), and the other notation is standard.

Shot 93 045 was an H-mode discharge with rather high upper and lower triangularity, and was fueled only by the neutral beam and was pumped to achieve 1 keV pedestal temperature. Shot 93 043 was a "companion" unpumped L-mode shot with high gas fueling over a period just prior to the time examined.

TABLE I. DIII-D shot parameters ($R=1.71-1.75$ m, $a=0.6$ m, $\kappa=1.74-1.84$, $I=1.0-1.6$ MA, $B=1.6-2.1$ T, LSN).

Shot(time) (ms)	*nebar* ($10^{19}/m^3$)	n_{ped} ($10^{19}/m^3$)	T_{eped} (eV)	q_{95}	δ	P_{nb} (MW)	Γ_{neut}^{in} (10^{20}/s)	f_{carb} (%)	τ_E (ms)	Confinement mode
93 045(3701)	4.7	4.0	1,093	4.08	0.45	5.1	0.3	2.0	195	H
93 043(2201)	9.5	6.9	281	3.56	0.33	4.7	1.4	2.8	186	L
97 979(3250)	7.9	6.4	524	3.94	0.75	6.5	0.6	2.0	238	H
98 893(4000)	12.5	8.0	119	2.95	0.13	2.1	2.5	1.0	166	H
92 976(3212)	6.0	4.7	187	5.72	0.33	5.0	3.8	1.0	70	H

The other three shots were "density limit" H-mode shots with a continuous high level of gas fueling. Shots 97 979 and 98 893 were able to maintain high pedestal densities and good H-mode confinement, while the H-mode confinement had deteriorated significantly in shot 92 976 at the time examined and it made a back H–L transition shortly afterwards. These shots had quite different triangularity and q_{95}.

A. Inferred transport coefficients

Average values of the temperature gradient scale lengths over the steep gradient pedestal region and over the "flattop" region extending inward several centimeters from the location of the top of the pedestal were determined *ab initio* from both the measured ion and electron temperature profiles. Average heat and particle fluxes were calculated in these regions, and the thermal diffusivities were then calculated from Eqs. (9) and (10). The results are given in Table II. Except for shot 93 045, the χ's in the steep gradient pedestal region were somewhat, but not greatly, smaller than the χ's in the flattop region, and this one exception is probably not significant. These χ's were used in the subsequent solution of the equations of the preceding section for the density and temperature profiles.

The range of values over each region of the main ion momentum transport frequency inferred *ab initio* from experiment by evaluating Eq. (13) are also given in Table II. In general, ν_{di}^* increased monotonically with radius at a rate greater than could be accounted for by atomic physics momentum loss rates. The values of ν_{dc}^* were also calculated, but they do not significantly affect the calculation.

The range of values over each region of the diffusion coefficients calculated from Eq. (5) are also shown in the table. It is emphasized that D's were evaluated during the course of the solution of the equations of the preceding section and not inferred *ab initio* from the experimental data, as the χ's and ν_{di}^* were. Although there does not appear to be any significant difference between the range of values of the diffusion coefficients in each region, the average value of the diffusion coefficients tended to be somewhat larger in the pedestal region than in the flattop region, due primarily to the larger values of ν_{iz} and ν_{di}^*.

B. Calculated and measured density and temperature profiles

The coupled set of nonlinear equations described in Sec. II were solved iteratively for the profiles of n_i, T_i, T_e, Γ_i, Q_i, Q_e, and n_o in the edge plasma. Experimental values for the radial electric field and the carbon toroidal and poloidal rotation velocities (as discussed in Sec. II A), experimental separatrix density and temperature boundary conditions, separatrix boundary conditions on particle and heat fluxes determined from particle and heat balances on the plasma, and a separatrix boundary condition on the neutral influx determined from a 2D neutral recycling calculation were used.

The principal results of these calculations for the five shot/time slices indicated in Table I are given in Figs. 1–5. Part (a) of Figs. 1–5 each shows the experimental E_r^{expt}, $v_{\varphi c}^{expt}$, and $v_{\theta c}^{expt}$ profiles that were used as input, and the profiles of the calculated v_{pinch} and $v_r=\Gamma_i/n_i$. It is clear from above

TABLE II. Transport coefficients inferred from experiment or calculated.

Shot (ms)	93 045(3701)	93 043(2201)	97 979(3250)	98 893(4000)	92 976(3212)
χ_{iped}[a] (m^2/s)	0.16	0.77	0.85	0.38	1.2
χ_{itop}[a] (m^2/s)	0.10	1.06	1.19	0.71	2.6
χ_{eped}[a] (m^2/s)	0.20	0.29	0.42	0.20	0.9
χ_{etop}[a] (m^2/s)	0.33	1.03	0.54	1.69	1.2
D_{iped}[b] (m^2/s)	0.47–0.69[c]	0.47–0.64	0.69–1.1	0.45–1.3	1.7–2.5
D_{itop}[b] (m^2/s)	0.44–1.1[c]	0.47–0.53	0.54–0.89	0.75–1.0	1.2–1.5
ν_{diped}[a] ($10^3/s$)	0.75–3.7[c]	1.24–2.10	2.8–5.3	8.0–19.0	1.3–11.3
ν_{ditop}[a] ($10^3/s$)	0.19–0.79[c]	0.04–0.92	0.08–2.3	0.7–5.8	0.58–1.2

[a]Inferred from experiment.
[b]Calculated.
[c]Range of values in region.

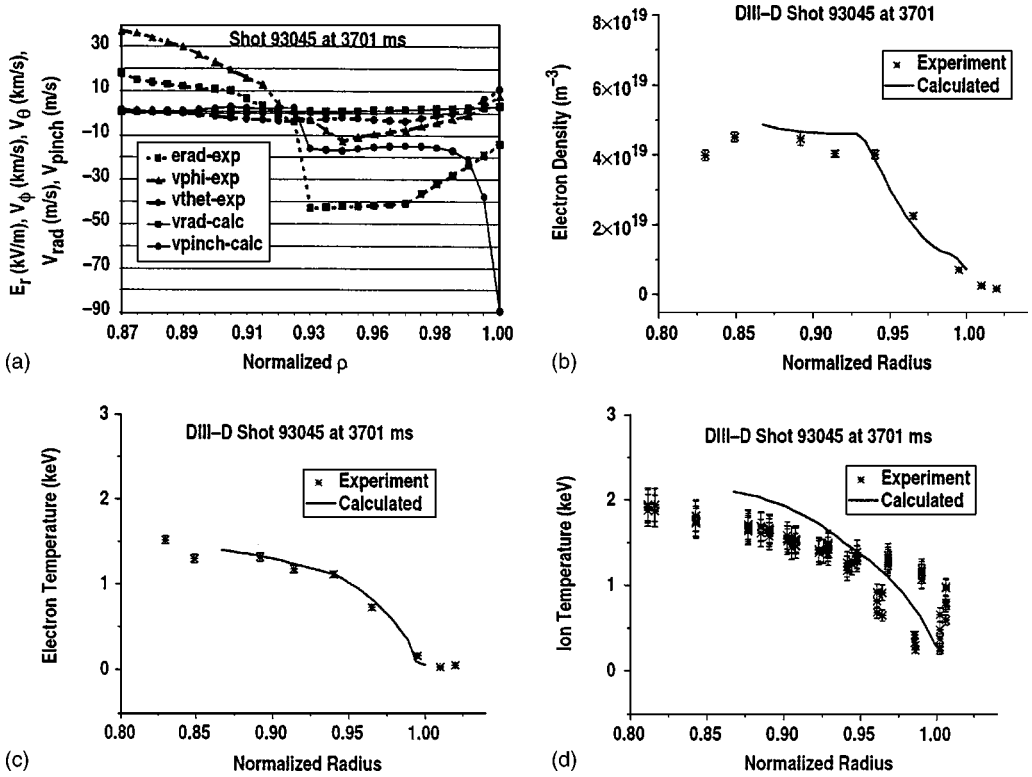

FIG. 1. Edge pedestal profiles for DIII-D H-mode discharge 93 045 calculated using experimental E_r, V_φ, V_θ, experimental separatrix boundary conditions, and experimentally inferred χ's: (a) quantities involved in calculating the pressure gradient, (b) calculated and measured n_e profiles, (c) calculated and measured T_e profiles, (d) calculated and measured T_i profiles.

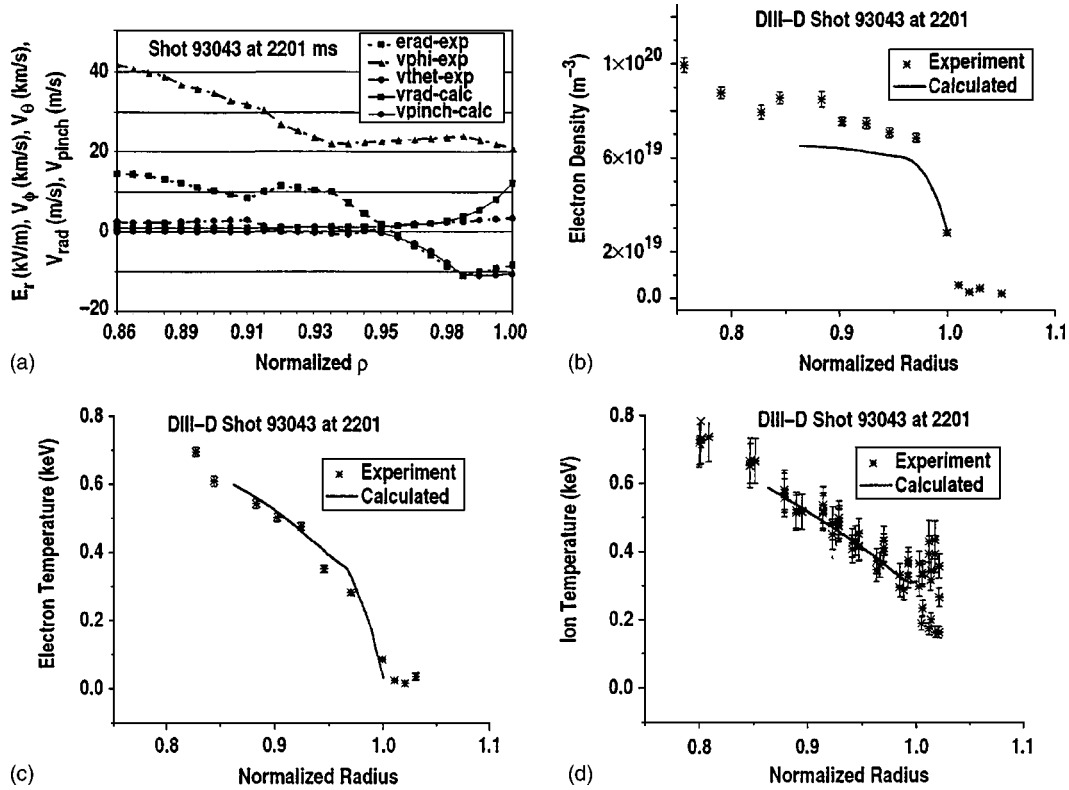

FIG. 2. Edge pedestal profiles for DIII-D H-mode discharge 93 043 calculated using experimental E_r, V_φ, V_θ, experimental separatrix boundary conditions, and experimentally inferred χ's: (a) quantities involved in calculating the pressure gradient, (b) calculated and measured n_e profiles, (c) calculated and measured T_e profiles, (d) calculated and measured T_i profiles.

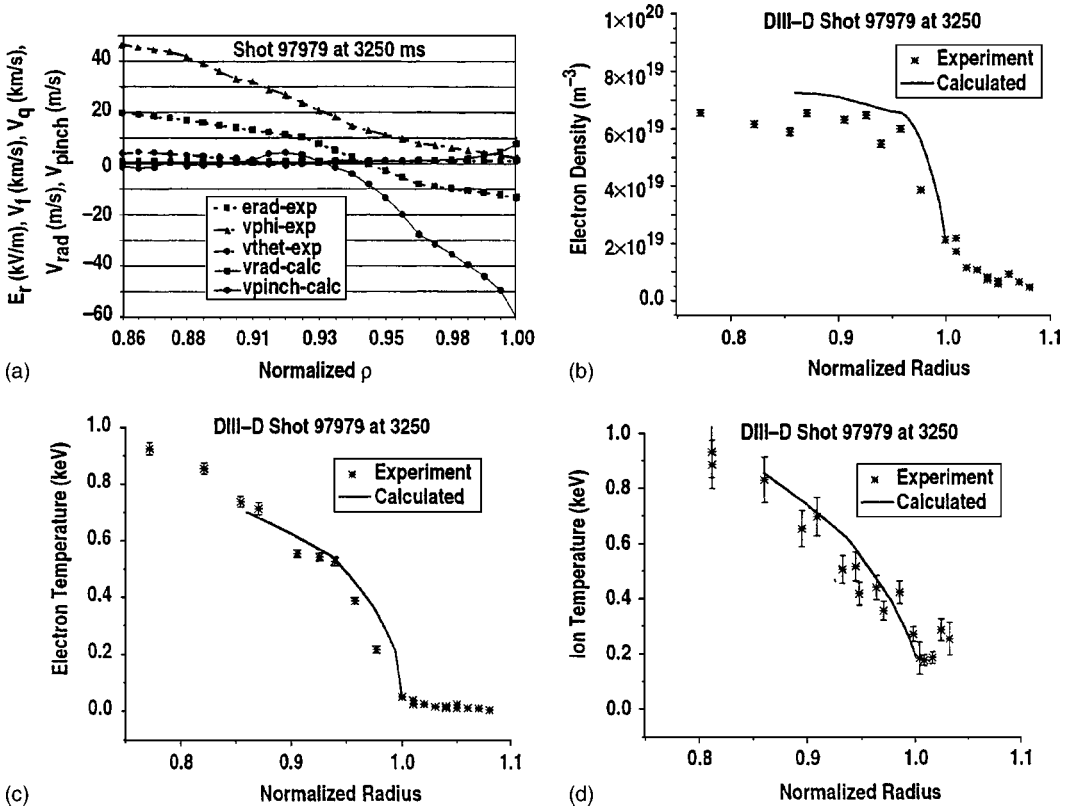

FIG. 3. Edge pedestal profiles for DIII-D H-mode discharge 97 979 calculated using experimental E_r, V_φ, V_θ, experimental separatrix boundary conditions and experimentally inferred χ's: (a) quantities involved in calculating the pressure gradient, (b) calculated and measured n_e profiles, (c) calculated and measured T_e profiles, (d) calculated and measured T_i profiles.

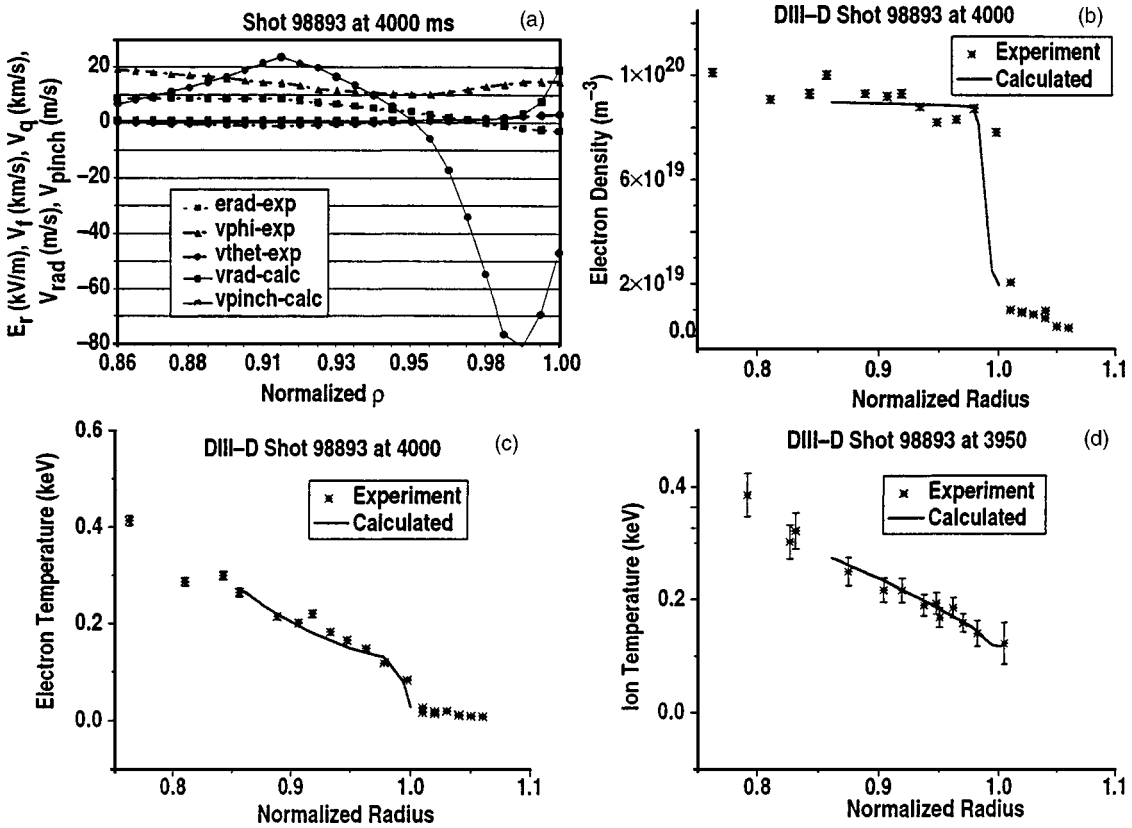

FIG. 4. Edge pedestal profiles for DIII-D H-mode discharge 98 893 calculated using experimental E_r, V_φ, V_θ, experimental separatrix boundary conditions, and experimentally inferred χ's: (a) quantities involved in calculating the pressure gradient, (b) calculated and measured n_e profiles, (c) calculated and measured T_e profiles, (d) calculated and measured T_i profiles.

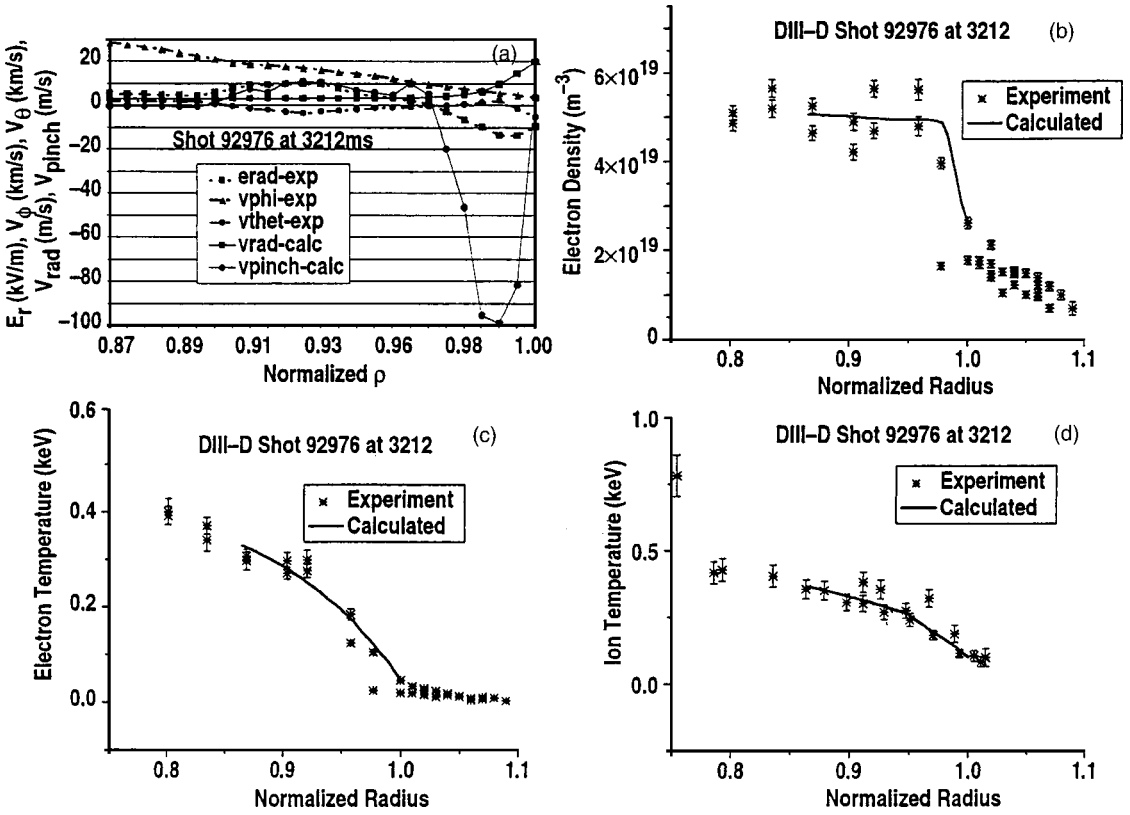

FIG. 5. Edge pedestal profiles for DIII-D H-mode discharge 92 976 calculated using experimental E_r, V_φ, V_θ, experimental separatrix boundary conditions, and experimentally inferred χ's: (a) quantities involved in calculating the pressure gradient, (b) calculated and measured n_e profiles, (c) calculated and measured T_e profiles, (d) calculated and measured T_i profiles.

mentioned figures and and Eq. (4) that the negative (inward) peaking of v_{pinch} just inside the separatrix produces (or at least is consistent with) a large negative pressure gradient just inside the separatrix. There is also a peaking of v_r just inside the separatrix, produced by the ionization of the fueling and recycling neutrals, that enhances the magnitude of the negative pressure gradient just inside the separatrix, but this atomic physics effect is not as large as the effect of the peaking in v_{pinch}.

Equation (6) can be examined for insight as to the cause of the peaking of v_{pinch} just inside the separatrix, but first it is convenient to use the radial force balance Eq. (12) in order to explicitly display the dependence on $v_{\varphi c}^{expt}$(c=z):

$$v_{pinch} = [-M_{\varphi i} - n_i e_i E_\varphi^A + n_i m_i (\nu_{iz} + \nu_{di}^*)(f_p^{-1} v_{\theta i} + E_r^{exp}/B_\theta) - m_i \nu_{iz} v_{\varphi c}^{expt}]/e_i B_\theta. \quad (15)$$

The first two terms (beam momentum input and induced toroidal field) are not important just inside the separatrix (although they become significant in the flattop region). Both ν_{iz} and ν_{di}^* increase with radius, the latter more dramatically just inside the separatrix. Examination of part (a) of Figs. 1–5 shows that there is a significant negative peaking of E_r^{expt} just inside the separatrix (except for 98 893 where the E_r^{expt} peaking is modest), which contributes to a negative v_{pinch}. There is also a positive peaking in $v_{\varphi c}^{expt}$ just inside the separatrix in shots 93 045 and 98 893, which contributes to a negative v_{pinch}. The behavior of $v_{\theta c}^{expt}$ just inside the separatrix is mixed among the shots.

The solution of Eq. (8) for the density profile exhibits a pedestal structure that agrees qualitatively with that found experimentally and is in reasonably good quantitative agreement with the experimental pedestal gradients and widths, as shown in part (b) of Figs. 1–5. With reference to Eq. (8), the steep density gradient in the edge pedestal is produced by an increase with radius of $v_{ri}=\Gamma_{ri}/n_i$ due to the ionization of incoming neutrals and to an increase with radius of the negative $v_{pinch,i}$ due to the negative peaking of E_r and $v_{\theta i}$ in the pedestal region. The value of the calculated diffusion coefficient D of Eq. (5) was not significantly different in the steep gradient pedestal region than in the flattop region on top of the pedestal, as shown in Table II, and did not play a significant role in determining the pedestal structure. This result confirms the finding of Refs. 26 and 27 over a range of edge conditions, namely, that given the observed negative peaking of E_r and $v_{\theta i}$ in the edge region, the pedestal structure of the edge density profile follows from the requirements of particle and momentum balances.

Similarly, the temperature profiles calculated from Eqs. (9) and (10) exhibit a pedestal structure and are in good agreement with measured profiles, but the interpretation of this result is not quite so straightforward as for the density pedestal. Because of an absence of knowledge of the thermal transport mechanisms, the χ's were inferred from experiment using $\chi_{av}=[Q_{av}/(n_{av}^{expt}T_{av}^{expt})-(5/2)\Gamma_{av}/n_{av}^{expt}]L_{T,av}^{expt}$. Average values of the density and temperature and of the temperature

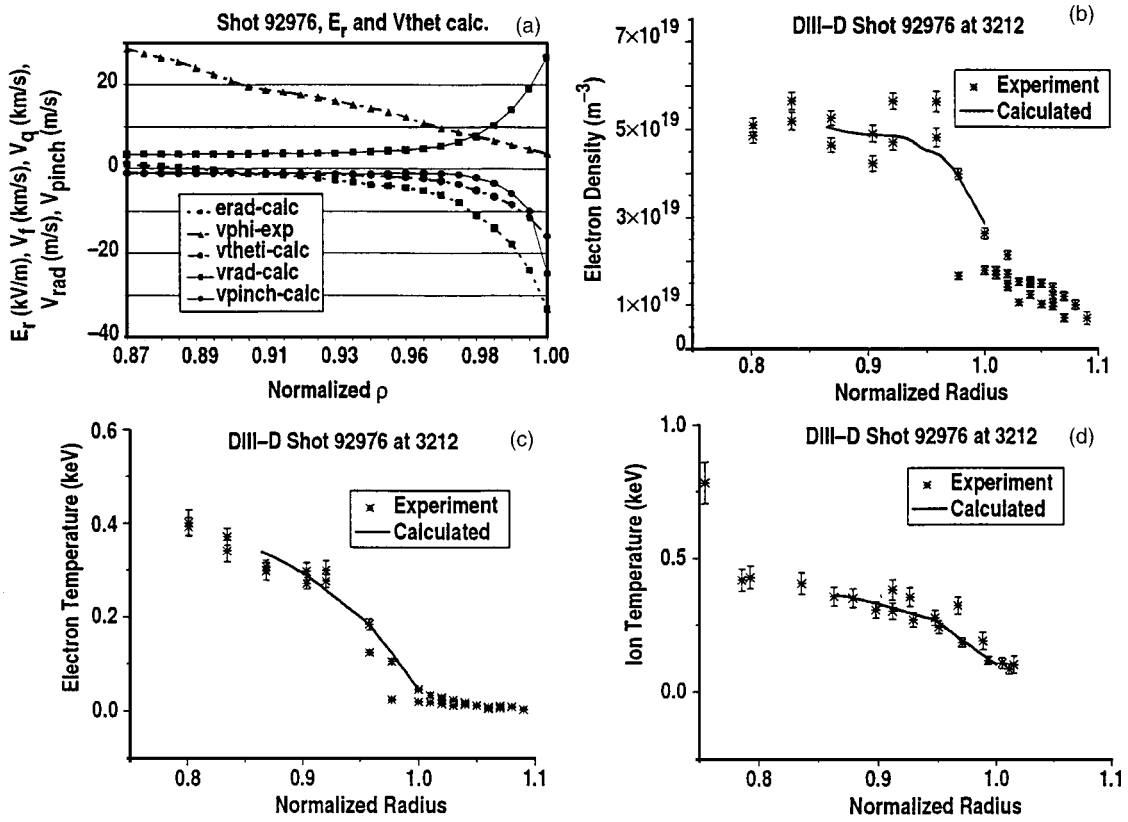

FIG. 6. Edge pedestal profiles for DIII-D H-mode discharge 92 976 calculated using only experimental V_φ, experimental separatrix boundary conditions and experimentally inferred χ's: (a) quantities involved in calculating the pressure gradient, (b) calculated and measured n_e profiles, (c) calculated and measured T_e profiles, (d) calculated and measured T_i profiles.

gradient scale length were determined from the experimental data, and average values of the heat and particle fluxes were determined from power and particle balances on the region inside the separatrix and corrected for edge atomic physics and radiation cooling and for ionization sources, separately in the steep gradient "edge pedestal" region and in the weak gradient flattop region.

The use of such average values inferred from experiment for the ion and electron χ's in the solution of the coupled set of Eqs. (1)–(3) and (7)–(11) did not predetermine the calculation of a temperature profile that agreed with experiment. The solutions of Eqs. (9) and (10) for the temperature profiles depended upon the solution of the coupled Eq. (8) for the density, which in turn depended on the solution of Eqs. (9) and (10) for the temperatures, and on the solutions of Eqs. (1)–(3) for the particle and heat flux profiles, and on the solutions to Eqs. (11) for the neutral density, etc., and these solutions were iterated to convergence.

The calculated temperature profile is determined by a number of factors. The temperature gradient is calculated from $-(dT/dr)=TL_T^{-1}=(Q-2.5\Gamma T)/n\chi$. The value of χ used in the calculation over the edge region of interest is a step function, as given in Table II, and by itself is only capable of producing linear temperature profiles with different slopes within the flattop and pedestal regions. Both the experimental and calculated temperature profiles generally have slopes which become steeper with increasing radius within both the flattop and the pedestal region, indicating (in the case of the calculated profile) that factors other than χ are involved in determining the profile.

With reference to the above formula for the slope of the temperature gradient, the total heat flux Q decreases slightly with radius because of atomic physics and radiation cooling, and the particle flux Γ increases sharply in the pedestal region because of ionization, as discussed previously. However, the effect of the sharp increase in Γ is partially offset by the sharp decrease in T with increasing radius. The density is almost constant in the flattop region, as shown in part (b) of Figs. 1–5, then decreases sharply with radius in the pedestal region. The resulting sharp and nonlinear decrease in the calculated T in the pedestal region [large and increasing with radius negative (dT/dr)] is correlated with the sharp decrease of n in the pedestal region.

The conclusion that can be drawn from the agreement between calculated and experimental density and temperature profiles shown in Figs. 1–5 is that, if the heat transport coefficients ($\chi's$) and the E_r and $v_{\theta i}$ in the pedestal region are known, then the particle, momentum, and energy balance equations and the heat conduction relationship [Eqs. (1)–(3) and (7)–(11)] are sufficient to determine the observed edge pedestal structure in the density and temperature profiles.

C. Uncertainties in experimental data

Any uncertainties in the determination of the experimental data enter directly into the evaluation of the gradient scale lengths of Eqs. (4) and (7). When the logarithmic derivative definitions of the gradient scale lengths are integrated inward from the separatrix, any uncertainty in gradient scale length resulting from uncertainty in experimental data unfortunately becomes amplified exponentially.

In the pedestal, the experimentally measured values of $v_{\varphi c}^{expt}$ and $v_{\theta c}^{expt}$ for the fully ionized carbon impurities have typical uncertainties of $\pm 1-2$ km/s due to photon statistics. These uncertainties increase as the carbon density drops and may reach values of $3-5$ km/s at the separatrix. In addition, there may be small systematic uncertainties, thought to be no greater than $\pm 1-3$ km/s, in obtaining the absolute wavelength reference needed for the rotation determination. There is also the potential for systematic errors due to interfering emission lines. The analysis attempts to account for these but they might add scatter comparable to the statistical uncertainties in some data. It is not expected that the velocities for the main ions are the same as velocities for the impurities. Thus, the main ion velocities can only be inferred from the impurity velocities with a model, such as is done in this paper. Such models have not been experimentally verified due to lack of measurements of main ion rotation in the edge.

D. Calculation of radial electric field and poloidal rotation velocities

The results of Figs. 1–5 indicate that the classical physics equations of Sec. II can predict the pedestal structure in density and temperature profiles, when the experimental values of the radial electric field and the rotation velocities are used to evaluate v_{pinch}. One of these calculations was repeated, but rather than using the experimental value of the radial electric field, the same radial force balance Eq. (12) that was used to calculate E_r^{expt} (using the experimental carbon rotation velocities $v_{\varphi c}^{expt}$ and $v_{\theta c}^{expt}$ and the experimental carbon pressure gradient) was used to calculate the radial electric field within the iterative solution of the equations of Sec. II. Since the main ion pressure gradient is the quantity calculated by these equations (the carbon pressure gradient scale length is assumed the same), E_r was in this case evaluated from Eq. (12) using the main ion $v_{\varphi i}^{expt}$ (determined from $v_{\varphi c}^{expt}$ as described in Sec. II A) and $v_{\theta i}$, and using the calculated L_{pi}^{-1}. To further relax the dependence of the calculation on experimental input, both $v_{\theta i}$ and $v_{\theta c}$ were calculated from poloidal momentum balance[26,27,36] as part of the iterative process. Thus, classical physics was used even more fully in the profile calculation for the evaluation of all quantities except for $v_{\varphi c}^{expt}$ (and the transport coefficients inferred from experiment). The results are given in Fig. 6.

Comparing Figs. 5(a) and 6(a), it is clear that the v_{pinch} profile near the separatrix is different in the two cases. The magnitude of v_{pinch} and v_r are comparable and the radial electric field and poloidal rotation velocity have a larger negative peaking just inside the separatrix when E_r and v_θ are calculated, resulting in a smaller value of the negative pressure gradient just inside the separatrix. This smaller pressure gradient produces a slope in the pedestal density profile that is in somewhat better agreement with experiment than when E_r and v_θ are taken from experiment [compare Figs. 5(b) and 6(b)].

The comparable importance of v_{pinch} and v_r in determining the pressure gradient just inside the separatrix implies a relatively larger role for the ionization of incoming neutrals (which causes the peaking in v_r) in determining the density gradient in the pedestal in Fig. 6 than was previously inferred from Fig. 5. A further indirect effect of the recycling and fueling neutrals comes about in the calculation of the results in Fig. 6 because v_r also contributed to the negative peaking of the calculated v_θ, which in turn contributed to the negative peaking of the calculated E_r and hence to the negative peaking of v_{pinch} just inside the separatrix. (It is not possible to trace these effects through the calculation when experimental values of E_r and v_θ are used in the calculation.)

IV. COMPARISON WITH RELATED WORK

The pedestal is an active topic of research, and a number of authors with varying objectives and approaches to the problem have contributed to the literature on the subject. It is useful to comment on a few representative examples of this literature vis-à-vis the present work in order to put the latter in perspective. First, it is the objective of this work to investigate the physical causes of the pedestal structure and, specifically, to test if the pedestal can be understood in terms of classical physics—particle, momentum, and energy conservation and the heat conduction relation—in the presence of recycling neutrals. For this reason, a number of perfectly reasonable procedures, such as correlating the pedestal structure to experimental results,[14] introducing heuristic models that reproduce certain observed features, etc. have been eschewed in favor of a rigorous solution of the equations that result from the first three-fluid moments equations and the heat conduction closure relation, in the presence of recycling neutrals.

There have been several models proposed to explain the observed dynamics of pedestal formation in terms of bifurcation in the transport properties,[15,16] orbit loss,[17] Stringer spin-up,[18] zonal flows,[19] etc. While some of the same physics is involved in this paper, the emphasis of this paper is on determining if the rigorous solution of the first three-fluid moment and the heat conduction equations have a solution with a pedestal structure when applied to calculate discharges that exhibit a pedestal structure experimentally.

A number of authors[15,20–27] have investigated the influence of the ionization of recycling neutrals (among other things) on the pedestal structure. It has been observed experimentally[21–23] and predicted theoretically[15,21,23] that the width of sharp-gradient edge pedestal region was comparable to the neutral ionization or penetration mean free path in the edge plasma. The calculations of this paper show that the ionization of recycling neutrals causes the negative ion pressure gradient to increase just inside the pedestal, contributing to a density pedestal in that location. The calculations of this paper show that an even larger contribution to the edge density pedestal is provided by the peaking of the inward pinch

velocity just inside the separatrix, due to a negative peaking of the radial electric field. However, further calculations (this paper and Refs. 26 and 27) showed that the ionization of recycling neutrals might be responsible, at least in part, for this negative peak in the radial electric field. Thus, there seems to be qualitative agreement between this paper and the previous papers that the ionization of recycling neutrals is important in determining the edge pedestal structure, although the physical models differ significantly.

Another fundamental investigation[25] of the physics of the edge pedestal came to a couple of conclusions similar to those of this paper, although the methodology was completely different. The edge of a tokamak plasma was analyzed with a particle guiding center code, including an X-point representation. Steep pedestal regions were found, and it was shown that they must be accompanied by a negative electric field peaking, consistent with the finding of the present paper. These authors also found that a sharply increasing convective ion loss towards the separatrix produced by the ionization of recycling neutrals, together with orbit squeezing and a X-point transport mechanism, were adequate to cause an edge pedestal. In the present paper it was also found that the increasing radial particle flux towards the separatrix (the v_r peaking) caused by neutral ionization was important in producing an edge pedestal, but that a particle pinch peaking near but inside the separatrix, rather than effects occurring outside the separatrix, was more important.

Finally, the pedestal region is usually simulated in the large edge physics codes by small diffusion and heat conduction coefficients modeled or adjusted to match experimental pedestal profiles (e.g., Refs. 28 and 29). A similar procedure is used in core-pedestal-SOL modeling codes (e.g., Ref. 30). The results of this paper, which indicate that it is the peaking in the pinch velocity rather than a sharp decrease in transport coefficient that produces the pedestal, would suggest that a different modeling procedure would be expected to better embody the underlying physics.

V. SUMMARY AND CONCLUSIONS

Balance equations for the radial particle (Γ_j) and heat (Q_j) fluxes and constraints that must be satisfied by the pressure and temperature logarithmic gradients, $L_{pj}^{-1} \equiv -(dp_j/dr)/p_j = (v_r - v_{pinch})/D$ and $L_{Tj}^{-1} \equiv -(dT_j/dr)/T_j = (Q_j - 2.5\Gamma T_j)/n_j T_j \chi_j$ in the plasma edge were derived from the first three-fluid moment equations—the particle, momentum, and energy balances—and from the heat conduction closure relations $q_j = -n_j \chi_j \, dT_j/dr$, $j = i, e$. Definitions of the particle transport coefficients, D and v_{pinch}, arose naturally in the derivation. These coupled nonlinear equations were numerically integrated inward from the separatrix, using separatrix boundary conditions determined from experiment and values of χ_j inferred from experiment, to calculate radial profiles of n_i, T_e, T_i, Γ_i, Q_i, and Q_e. The calculation of the neutral particle density n_o, which was needed to evaluate the atomic physics particle source and heat losses, was iterated to consistency with the plasma density and temperature profiles.

This calculation process was applied to calculate the radial profiles of density and temperature in the edge of 5 DIII-D discharges embodying a wide range of edge conditions and plasma parameters. The values of the radial electric field and the toroidal and poloidal rotation velocities needed to evaluate v_{pinch} were taken from experiment. The calculated density and temperature profiles in the plasma edge exhibited a definite pedestal structure, in agreement with the profiles measured in these discharges. A peaking of the inward (negative) v_{pinch} just inside the separatrix was identified as the principal cause of the strong negative pressure gradient just inside the separatrix, and hence of the observed density pedestal, in these discharges. The peaking of the radial velocity $v_r = \Gamma_i/n$ just inside of the separatrix caused by the ionization of recycling and fueling neutrals was identified as a secondary contributor to the observed strong negative pressure gradient just inside the separatrix.

The two principal conclusions indicated by these results are (1) if the heat transport coefficients ($\chi's$) and the E_r and $v_{\theta i}$ in the pedestal region are known, then the particle, momentum, and energy balance equations, the heat conduction relationship, and the neutral particle transport equations [Eqs. (1)–(3) and (7)–(11)] are sufficient to determine the observed edge pedestal structure in the density and temperature profiles in the edge of H-mode tokamak plasmas; and (2) the major cause of the edge pedestal structure in the density profile is the large peaking in v_{pinch} just inside the separatrix. The pinch velocity is caused primarily by the rotation velocity and the radial electric field; thus the remaining questions in understanding the pedestal structure would seem to be related to the causes of the observed rotation velocities and radial electric field in the edge plasma and to the heat transport mechanisms in the edge pedestal.

The calculation for one discharge was repeated with the radial electric field and poloidal rotation velocities also being calculated from momentum balance. The calculated profiles were in somewhat better agreement with the measured profiles than when the experimental values of the radial electric field and poloidal rotation velocities were used in the calculation. Thus, it may well be that both the density and temperature profile pedestal structure and the associated radial electric field and rotation velocity profiles in the plasma edge are natural consequences of classical physics particle, momentum, and energy conservation and the heat conduction relations—but this remains to be established by a more extensive investigation.

ACKNOWLEDGMENTS

This work was supported by the U. S. Department of Energy under Grant No. DE-FG02-00-ER54538 with the Georgia Tech Research Corporation and by U. S. Department of Energy under Contract No. DE-AC03-99ER54463 with General Atomics Co. W.M.S. is grateful to General Atomics for their hospitality during the course of this work.

[1] A. E. Hubbard, Plasma Phys. Controlled Fusion **42**, A283 (2000).
[2] M. Kotschenreuther, W. Dorland, Q. P. Liu *et al.*, *Proceedings of the 16th Conference Plasma Phys. Control Fusion Research, Montreal, 1996* (IAEA, Vienna, 1997), Vol. 2, p. 371.

[3]J. E. Kinsey, R. E. Waltz, and D. P. Schissel, Proceedings of the 24th EPS, Berchtesgarten 1997, Vol. III, p. 1081.
[4]R. L. Miller, Y. R. Lin-Liu, T. H. Osborne, and T. S. Taylor, Plasma Phys. Controlled Fusion **40**, 753 (1998).
[5]J. W. Connor, R. J. Hastie, H. R. Wilson, and R. L. Miller, Phys. Plasmas **5**, 2687 (1998).
[6]H. R. Wilson and R. L. Miller, Phys. Plasmas **6**, 873 (1999).
[7]B. N. Rogers and J. F. Drake, Phys. Plasmas **6**, 2797 (1999).
[8]P. B. Snyder, H. R. Wilson, J. R. Ferron *et al.*, "Modification of high-mode pedestal instabilities based on coupled peeling-ballooning modes," Phys. Plasmas **9**, 2037 (2002).
[9]P. B. Snyder, H. R. Wilson, J. R. Ferron *et al.*, Nucl. Fusion **44**, 320 (2004).
[10]R. J. Groebner and T. H. Osborne, Phys. Plasmas **5**, 1800 (1998).
[11]T. H. Osborne, J. R. Ferron, R. J. Groebner *et al.*, Plasma Phys. Controlled Fusion **42**, A175 (2000).
[12]W. Suttrop, O. Gruber, B. Kurzan *et al.*, Plasma Phys. Controlled Fusion **42**, A97 (2000).
[13]J. R. Ferron, M. S. Chu, G. L. Jackson *et al.*, Phys. Plasmas **7**, 1976 (2000).
[14]T. Onjun, G. Bateman, A. H. Kritz *et al.*, Phys. Plasmas **9**, 5018 (2002).
[15]F. L. Hinton and G. M. Staebler, Phys. Fluids B **5**, 1281 (1993).
[16]W. M. Stacey, Phys. Plasmas **9**, 3082 (2002).
[17]K. C. Shaing and E. C. Crume, Phys. Rev. Lett. **63**, 2369 (1989); K. C. Shaing, E. C. Crume, and W. A. Houlberg, Phys. Fluids B **2**, 1492 (1990).
[18]A. B. Hassam, T. M. Antonsen, J. F. Drake, and C. S. Lui, Phys. Rev. Lett. **66**, 309 (1991).
[19]P. N. Gudzar, R. G. Kleva, R. J. Groebner, and P. Gohil, Phys. Plasmas **11**, 1109 (2004).
[20]W. M. Stacey, Phys. Plasmas **8**, 4073 (2001).
[21]R. J. Groebner, M. A. Mahdavi, A. W. Leonard *et al.*, Phys. Plasmas **9**, 2134 (2002).
[22]W. M. Stacey and R. J. Groebner, Phys. Plasmas **10**, 2412 (2003).
[23]R. J. Groebner, M. A. Mahdavi, A. W. Leonard *et al.*, Nucl. Fusion **44**, 204 (2004).
[24]W. M. Stacey, Phys. Plasmas **11**, 1511 (2004).
[25]C. S. Chang, S. Ku, and H. Weitzner, Phys. Plasmas **11**, 2649 (2004).
[26]W. M. Stacey, "Structure of the edge density pedestal in tokamaks," Phys. Plasmas **11**, 4295 (2004).
[27]W. M. Stacey, "Edge pedestal structure," Phys. Plasmas **11**, 5487 (2004).
[28]G. D. Porter, R. Isler, J. Boedo, and T. D. Rognlien, Phys. Plasmas **7**, 3663 (2000).
[29]A. Kallenbach, Y. Andrew, M. Beurskens *et al.*, Plasma Phys. Controlled Fusion **46**, 431 (2004).
[30]G. W. Pacher, H. D. Pacher, G. Janeschitz *et al.*, Plasma Phys. Controlled Fusion **46**, A257 (2004).
[31]W. M. Stacey, Phys. Plasmas **4**, 179 (1997).
[32]W. M. Stacey and J. Mandrekas, Nucl. Fusion **34**, 1385 (1994).
[33]W. M. Stacey, Nucl. Fusion **40**, 965 (2000).
[34]R. J. Colchin, Nucl. Fusion **40**, 175 (2000).
[35]W. M. Stacey, Phys. Plasmas **5**, 1015 (1998); **8**, 3673 (2001).
[36]W. M. Stacey, Phys. Plasmas **9**, 3874 (2002).